NASA-TM-106999

NASA Technical Memorandum 106999
AIAA–95–3037

Inlet Flow Test Calibration for a Small Axial Compressor Rig: Part II. CFD Compared With Experimental Results

D.P. Miller
Lewis Research Center
Cleveland, Ohio

and

P.S. Prahst
NYMA, Inc.
Brook Park, Ohio

Prepared for the
31st Joint Propulsion Conference and Exhibit
cosponsored by AIAA, ASME, SAE, and ASEE
San Diego, California, July 10–12, 1995

National Aeronautics and
Space Administration

Inlet Flow Test Calibration for a Small Axial Compressor Rig Part II. CFD Compared with Experimental Results

D. P. Miller†
NASA Lewis Research Center
Cleveland, OH 44135

P. S. Prahst‡
NYMA, Inc.
Cleveland, OH 44135

Abstract

An axial compressor test rig has been designed for the operation of small turbomachines. A flow test was run to calibrate and determine the source and magnitudes of the loss mechanisms in the compressor inlet for a highly loaded two-stage axial compressor test. Several flow conditions and IGV angle settings were established, which detailed surveys were completed. Boundary layer bleed was also provided along the casing of the inlet behind the support struts and ahead of the IGV. Several CFD calculations were made for selected flow conditions established during the test. Good agreement between the CFD and test data were obtained for these test conditions.

1.0 Introduction

NASA Lewis Research Center has several facilities dedicated to compressor research. One of the facilities dedicated to small compressor research is the SECTF[1], Small Engine Components Test Facility. The facility, shown in Figure 1, was designed to handle flows up to 30 kg/s, a maximum pressure ratio of 30:1, provides a maximum speed of 60,000 rpm and produces a maximum shaft power of 4474 kW. Compressor inlet air can be varied from 1.37×10^4 to 3.45×10^5 Pa and the air temperature can vary from ambient to -57 C. The test was conducted using atmospheric inlet conditions.

A joint cooperative program with Allison Engine Company was established to run a small highly loaded axial compressor in the facility. In order to establish a baseline flow through the inlet which will be used for the compressor test, a flow test without the compressor was conducted to survey the inlet region ahead of the compressor face. Details of the flowpath design and test data were presented in Part I: Design and Experimental Results[2].

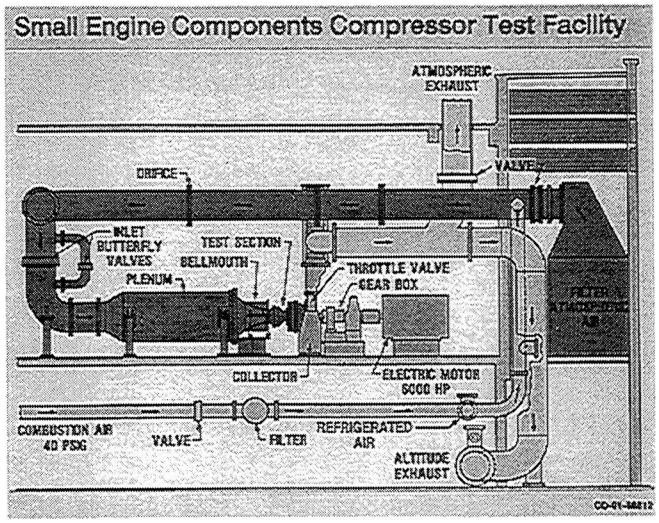

Figure 1: CE18 Test Facility at NASA Lewis

Several analyses were compared with the test data. Axisymmetric throughflow and full 3-D solutions were obtained using ADPAC at various flow rates, IGV flap angle settings and bleed conditions. ADPAC is a four stage Runge-Kutta finite volume multi-block Navier-Stokes flow solver with a Baldwin-Lomax turbulence model.

†Research Engineer
‡Member ASME

Details of the code development can be found in references 3,4,5,6 and 7. Since the compressor operation required different flap settings as the compressor was throttled to full speed along a given operation line, the test had several conditions at which measurements were obtained.

2.0 Flow Test Conditions

The following set of test conditions were used to compare the CFD to the flow measurements.

Table 1: Range of Flow Test Conditions

$\dot{m}\sqrt{\theta}/\delta$ kg/sec	IGV α Degrees	%Bleed
3.86	0.0	0.0
3.88	0.0	2.0
3.88	11.0	1.0
3.29	30.0	0.0
2.77	40.0	0.0

Where

$\dot{m} \equiv$ Mass Flow

$\theta \equiv T_0 / T_{0std}$

$\delta \equiv P_0/P_{0std}$

$\alpha \equiv$ Angle in Degrees

2.1 Computational Modeling

As mentioned in part I; a miniature traversing cobra probe was designed to complete a circumferential traverse behind the IGVs over a 72 degree circumferential travel. Detailed surveys were made to determine the contribution by five Small Support Struts, five Main Support Struts, 26 IGVs and five Inlet Rakes (see Figure 2). The small support struts were fourteen chord lengths upstream of the IGV and the measurements indicated the wakes from the struts had mixed out by the time they reached the measurement plane. Since the measured data indicated no significant contribution, the small support struts were not modeled as part of the CFD. As far as considering the contributions of the main support struts, the losses were measurable, but were found to be relatively small, therefore, in order to simplify the computations, the main support struts were excluded in the calculations. It is extremely difficult to completely model the inlet rakes, therefore, the CFD computations have modeled only the IGV and upstream duct with no inlet rakes.

3.0 CFD Compared to Experiment

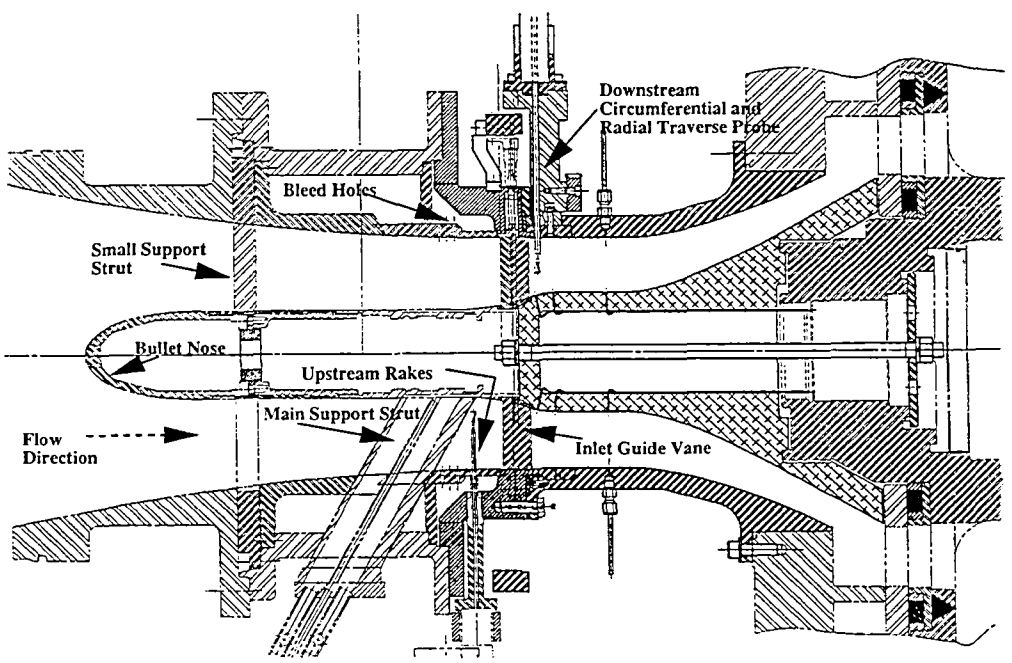

Figure 2: Cross Sectional View of the Cold Flow Configuration

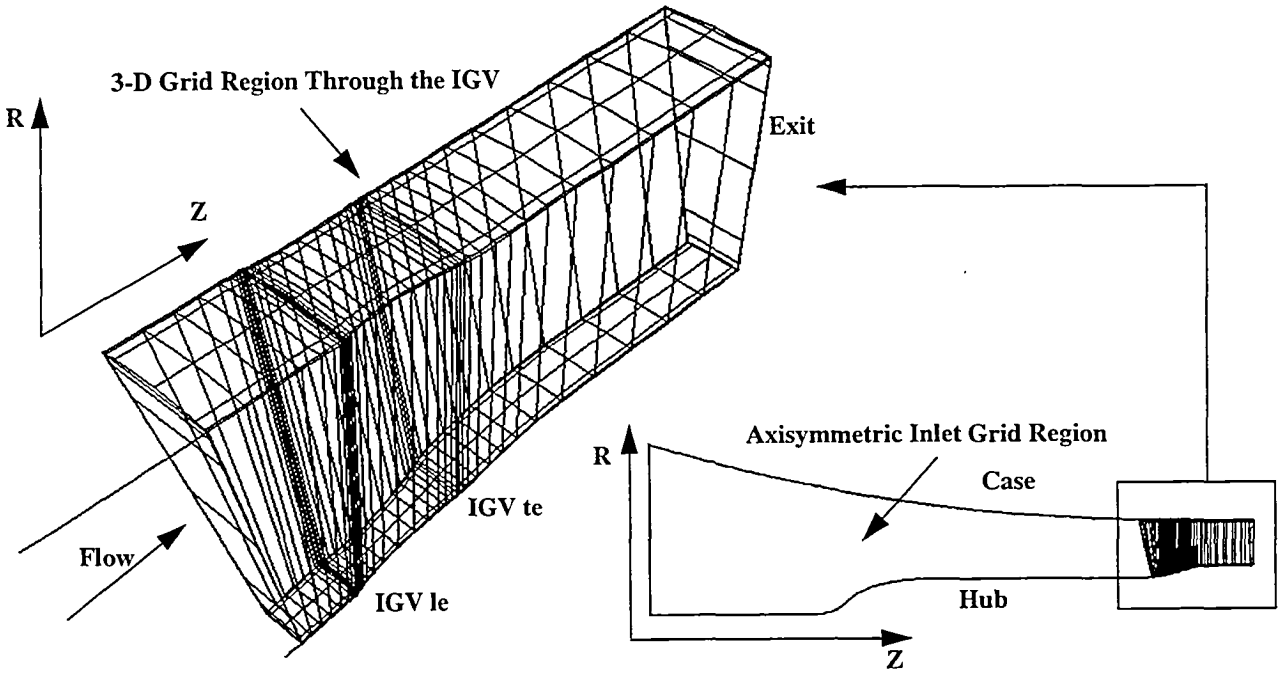

Figure 3: Grid Layout Used for the 3-D Flow Field Solutions

The CFD solutions will be shown in 3 parts. The first part will be a comparison of the axisymmetric throughflow to the 3-D solution at mid-pitch; the second part will show the blade-to-blade computations compared with the 3-D solutions at mid-span. Finally, the 3-D computations compared to the measurement plane behind the IGV.

3.1 Computational Grids

The flow computations were done on H and C type grids generated by TIGGC3D[8-9]. ADPAC was developed to allow flows to be computed with multi-block grids; the H-grids used to compute the 3-D flow fields were divided into two block regions where the inlet ahead of the IGV was gridded axisymmetrically and then a full 3-D grid was used for the IGV and exit region (see Figure 3). The computations were done at 4 different flap angles, 0, 11, 30 and 40 degrees. The H-grid used for the zero IGV flap setting consisted of 153x49x1 in the inlet region and 145x49x49 grid in the IGV region for a total of 355,642 grid points. For the 30 degree IGV flap angle setting the same H-grid in the inlet was used and 165x49x49 for the IGV for a total of 403,662 grid points. The number of axial points was increased in the IGV region to try and resolve any separation that might exist between the strut portion and the flap. For the 11 and 40 degree flap angle settings, the H-grids consisted of 113x49x1 for the inlet and 145x49x49 for the IGV region for a total of 353,682 grid points. From the previous studies at the zero and 30 degree

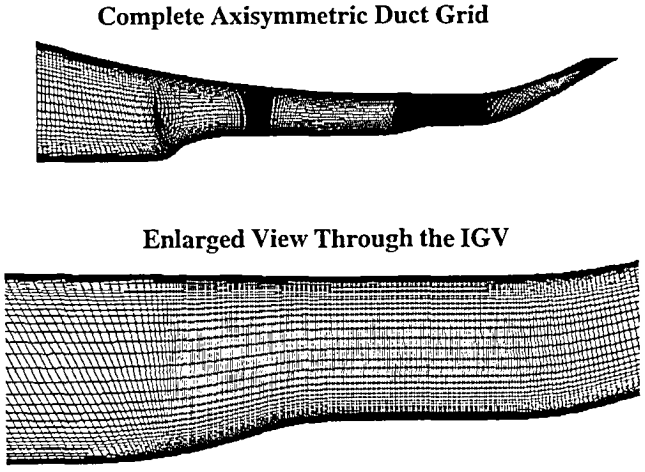

Figure 4: Axisymmetric Grid Used in the CFD Solution

flap settings, much of the upstream grid was reduced without affecting the resolution of the boundary layer coming into the IGV. For the axisymmetric solution, the H-grid used on the entire flowtest duct was a 481x81x1, shown in Figure 4, to resolve the flow field in the duct through the IGV and the exit region.

The second part of the CFD study consisted of a 2-D blade-to-blade computations which were computed at the 50% spanwise location for the IGV at 0, 11, 25, 30, 40 and

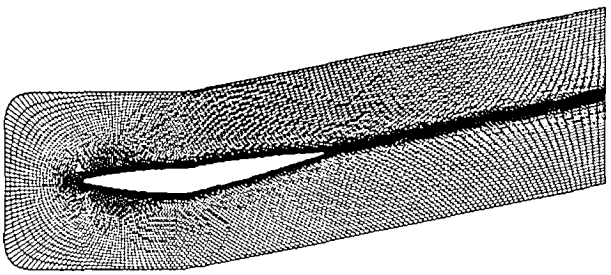

Figure 5: C-Grid Around the IGV set at an 11° Flap Angle

45 degree IGV flap angle settings. All the grids used were identical C-grids of 281x49 grid points (Figure 5). The 2-D solutions were used to compare with the 3-D at mid-span and the losses for each angle setting with the measured data.

All the solutions were run on high speed workstations, primarily a Silicon Graphics™ Power Challenge. The 2-D solutions took approximately 3500 iterations and 40 minutes wall clock time to reach convergence. The 3-D solutions took approximately 1600 iterations and a little over 18 hours wall clock time to reach convergence.

3.2 Axisymmetric CFD Compared to 3-D CFD and Test Data

Figure 6 shows the axisymmetric throughflow and the 3-D solution at mid-gap compared at nominal conditions, 3.86kg/sec, 0 degree flap angle setting and no bleed. They are in good agreement up to the IGV. The axisymmetric solution presented does not include any forces or blockage associated with the IGV which accounts for the differences between the solutions. Both the axisymmetric and the 3-D computations were compared to the radial surveys taken mid-pitch between the IGVs,. Figure 7 shows a comparison

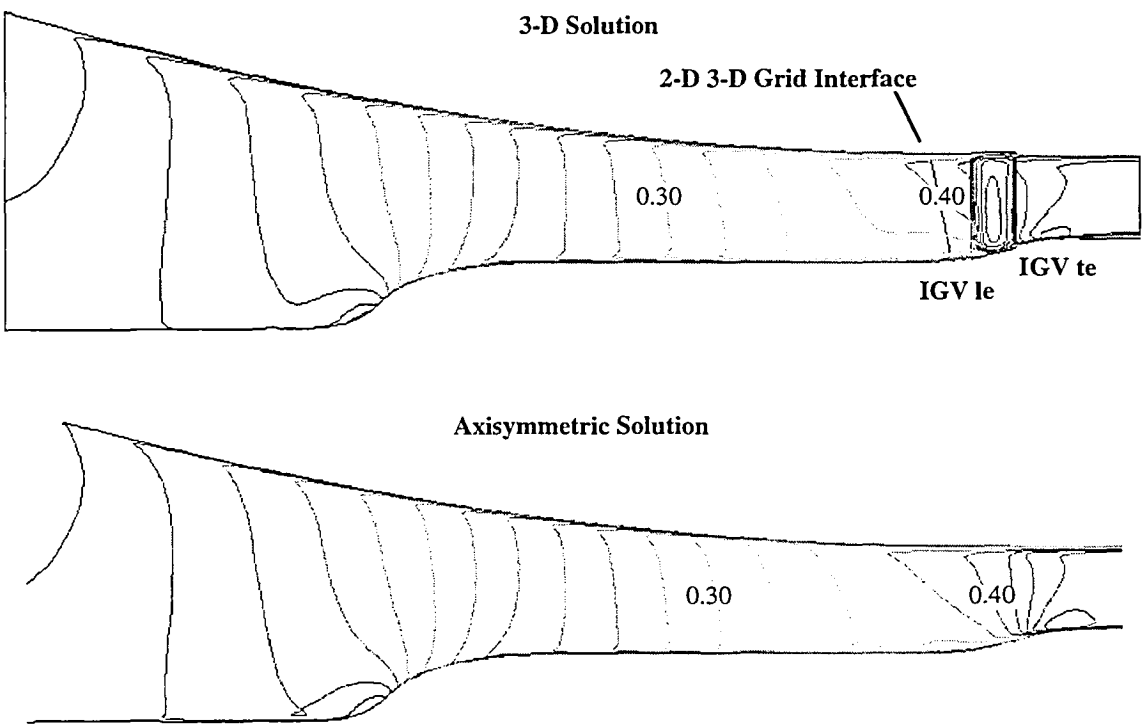

Figure 6: Axisymmetric View of the CFD Solutions

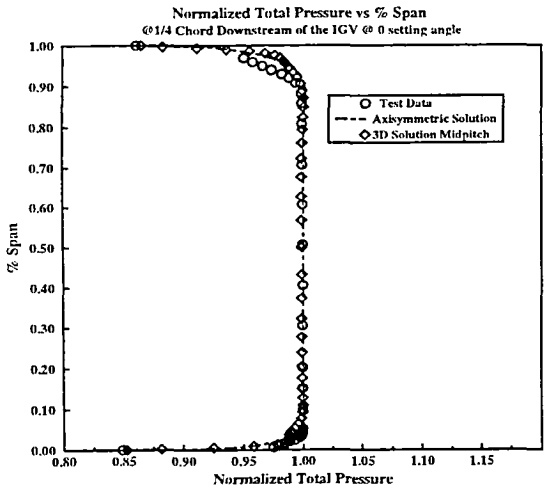

Figure 7: CFD Compared to Measured Radial Profile 3.86kg/s at 0% Bleed and IGV at 0°

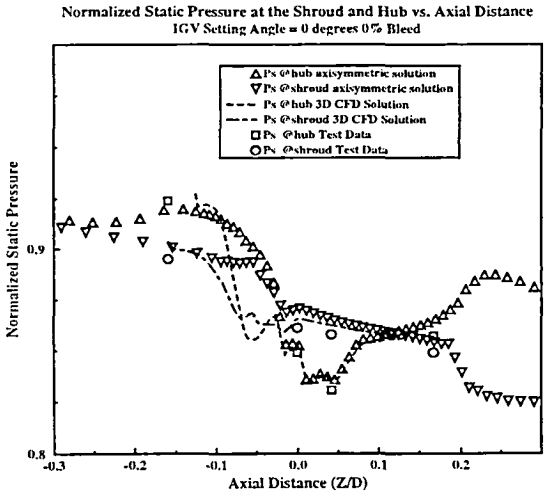

Figure 8: Comparison of Wall Static Pressure vs. Test Data

of the radial profile measured behind the IGV, they are in very good agreement to test conditions with exception of the region about 10% span near the casing. The error is a result of the cobra probe and the hole in the casing having an influence on the boundary layer; the hole in the casing and the probe produced additional blockage into the boundary layer which causes the probe to read a lower total pressure. Even though the two CFD models are slightly different than the test data, they agree quite well with each other.

Looking at the static pressure comparisons, as shown in Figure 8, the computations match the data fairly well. The 3-D CFD solutions matches the data slighter better due to the presence of the IGV in the solution. The computed mass flows for the axisymmetric and 3-D solutions were 3.88 kg/sec and 3.83 kg/sec which represented 0.5%- 0.7% error in mass flow from the 3.86kg/sec measured in the test. The mass flow was slightly lower for the 3-D solution.

The flowtest was also run with casing boundary layer bleed to reduce the blockage to what a compressor would experience during normal operation. ADPAC was developed with the feature to bleed flow from a boundary, therefore, the CFD calculation was also done with 2% bleed flow. Bleed for the CFD solution was imposed ahead in the axisymmetric mesh, that was were the bleed holes are physically located axially in the casing (refer to Figure 2). The bleed location was set at a couple of grid points to approximate the same physical axial location in the casing.

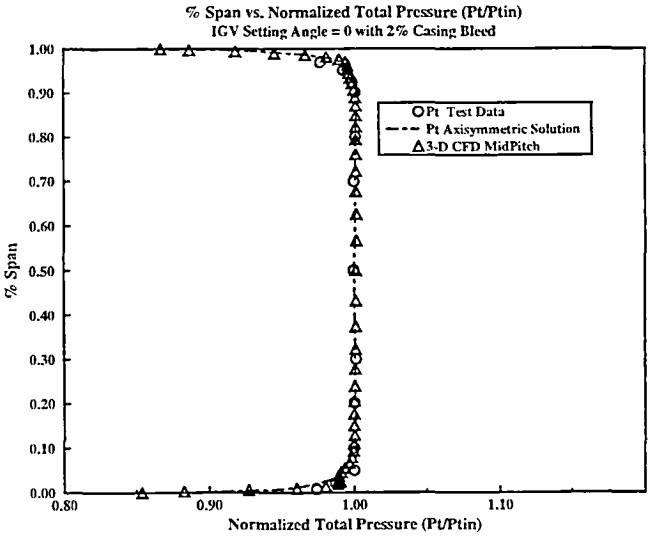

Figure 9: CFD Compared to Measured Radial Profile 3.86kg/s at 2% Bleed and IGV at 0°

Figure 9 shows the radial total pressure profile differences between the CFD analysis with the test results at 3.86kg/sec, 0 degree IGV flap angle setting and 2% bleed. The results are in quite good agreement even near the casing where the probe end interacts with the hole in the casing. The effective blockage was significantly reduced by bleeding the boundary layer ahead of the IGV. Unfortunately, the bleed occurs about 1 chord ahead of the IGV, which still allows for some redevelopment of the

boundary layer. Bleed in ADPAC is actually applied at cell faces at grid point(s) along the boundary allowing for redevelopment of the boundary layer, which would account for such good agreement between the solutions and the data.

The static pressure comparisons for the 2% bleed are shown in Figure 10. The CFD solutions match the data very well. Again, the 3-D solution matches better than the axisymmetric solution because of the inclusion of the IGV in the modeling. The computed mass flows for the axisymmetric and 3-D solutions with bleed were 3.89 kg/sec and 3.84 kg/sec which represented 0.25%-1.0% error in then mass flow to 3.86 kg/sec measured in the test.

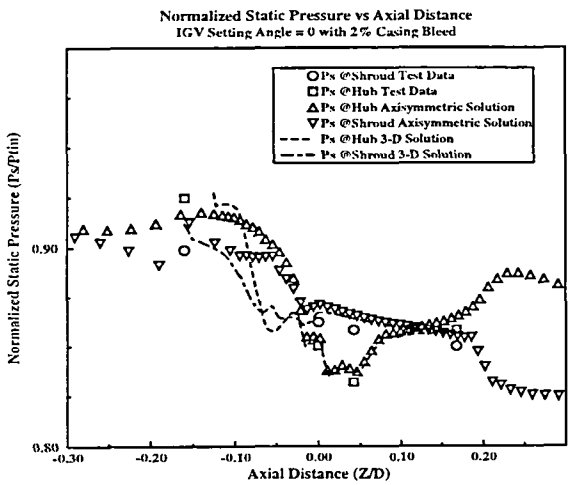

Figure 10: Comparison of the Wall Static Pressure at 2% Bleed Flow

3.3 CFD Blade-to-Blade Computations compared to 3-D Mid-Span

2-D blade-to-blade computations were done at the IGV mid-span to determine the loss over a range of flap angle settings. The blade-to-blade calculations were easy to compute with a short turn around time. This was extremely useful in trying to understand why the test results had indicated a significant increase in the losses at the higher IGV flap angle settings. The IGV was composed of a strut and a flap, but the IGV geometry for all of the 2-D Blade-to-Blade CFD analysis was modeled as a continuous airfoil.

The blade-to-blade calculations were computed in order to give guidance to the full 3-D solutions. From the data, there was an apparent increase in the losses as the IGV was set to

2-D Blade-to-Blade Solution

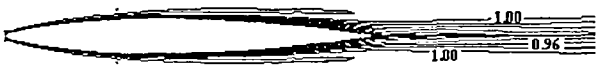

3-D Solution at Mid-Span

Figure 11: Comparisons of Total Pressure Between the 2-D and 3-D solutions at 0 Degrees.

2-D Blade-to-Blade Solution

3-D Solution at Mid-Span

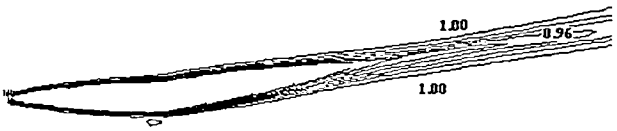

Figure 12: Comparisons of Total Pressure Between the 2-D and 3-D solutions at 11 Degrees.

higher flap angle settings. Thus, in order to evaluate the CFD, the total pressure distributions for the 2-D blade-to-blade computations are compared with the 3-D solutions in Figures 11 and 12 at flap angles of 0 and 11 degrees. The CFD computations agreed quite well. Actually, the blade-to-blade solutions were slightly higher in loss than the 3-D.

The blade-to-blade computation was then run with the flap set at 30 degrees. From the test data, the losses were known to increase significantly. However, the 2-D solution had only indicated a very modest change in the wake profile (Figure 13). It was believed that at the higher flap

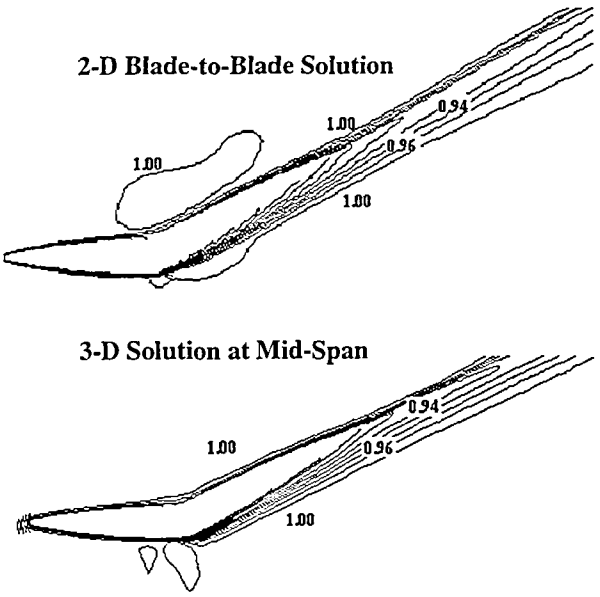

Figure 13: Comparisons of Total Pressure Between the 2-D and 3-D solutions at 30 Degrees.

angle settings, the airfoil would separate on the suction side of the airfoil increasing the losses substantially. Since the higher losses weren't indicated by the 2-D solutions, a full 3-D solution was then computed. The 3-D solution compared fairly well with the 2-D (see Figure 13), but did not indicate a large wake developing behind the IGV.

As mentioned earlier, the losses obtained from the test data had indicated larger wakes at this flap angle setting than what was computed. The computational model had been derived by using a continuous airfoil section from leading to trailing edge, but the IGV geometry was really a strut followed by a flap with a small gap between the strut and the flap. The 2-D airfoil and grid model was modified (as shown in Figure 14) to look similar to a strut with the flap behind the strut set at the 30 degree angle. The wake generated in the strut-flap 2-D model had significantly changed over the continuous airfoil 2-D solution (see Figure 15). The computation clearly indicated that the strut-flap combination was clearly higher in loss than the original airfoil. A review of the geometry as built in the test was conducted to determine what modification of the model was needed for the 3-D CFD calculation.

As indicated before, the strut and flap were actually two separate airfoils with a small gap between the two. The gap between the strut and flap was very small, in the order of a few millimeters, and to grid the gap would be difficult. Fortunately, ADPAC was written such that flow could be

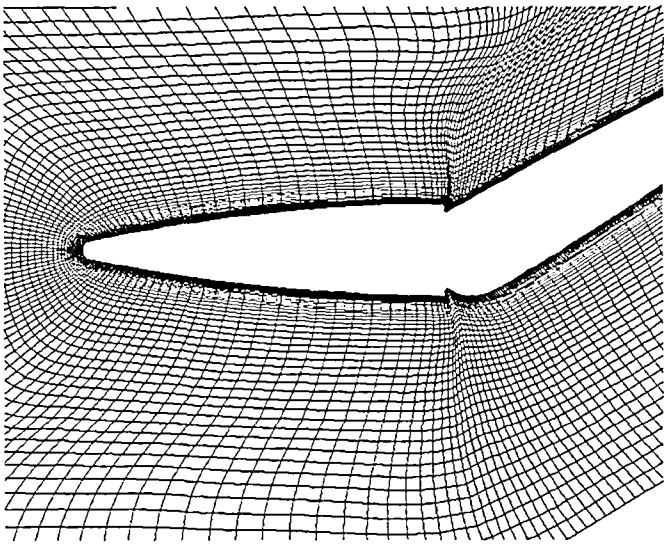

Figure 14: Modified 2-D Strut-Flap Combination for the IGV Geometry and Grid at a 30° Flap Angle

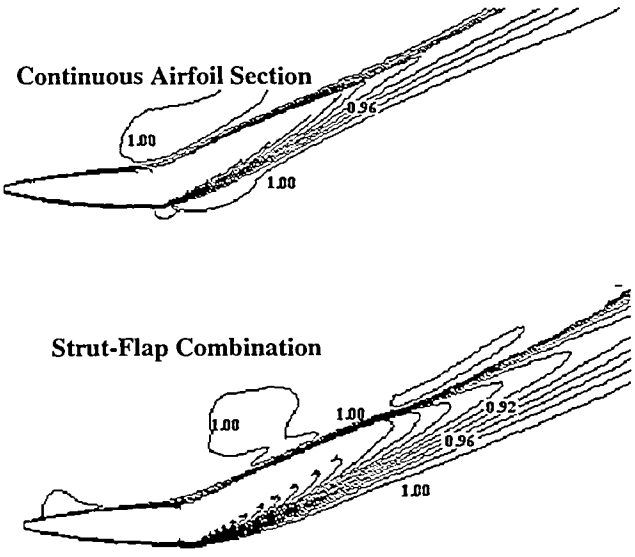

Figure 15: Comparison of the Total Pressure of the 2-D IGV Strut-Flap and the 2-D Continuous Airfoil Section

leaked from the pressure side of the airfoil to the suction side in the boundary condition specification. A finer 3-D axial grid was generated and the flow was allowed to leak at 2 grid points near the joint between the strut and the flap. This is an approximation of the gap between the strut and the flap. The two points where the flow was allowed to leak

was in all probability larger than the true gap, but this provided a way to model the flow without having to grid the true gap.

When the flow was allowed to leak through the gap, the 3-D CFD solution showed a similar increase in the total pressure loss behind the strut. The total pressure contours for the 2-D strut-flap and 3-D flow with the leakage are compared in Figure 16. The wake is slightly larger in the 3-D solution.

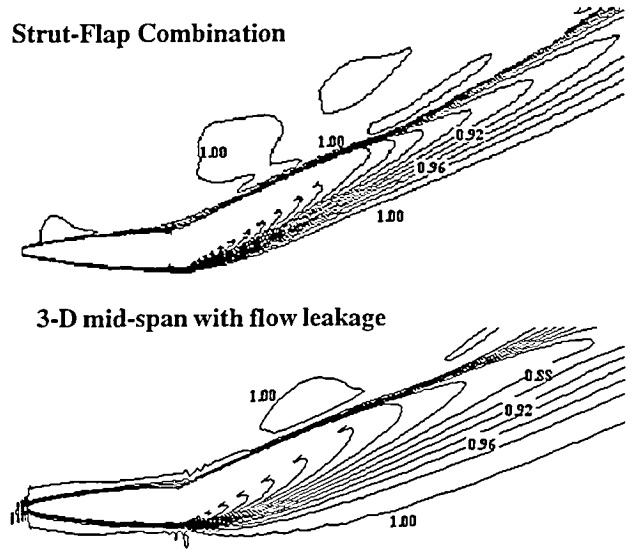

Figure 16. Comparison of Total Pressure Contours between the 2-D Strut-Flap and 3-D at Mid-Span with Leakage Flow through the Gap

3.4 Loss Calculations

Losses from the test data, 2-D blade-to-blade CFD and 3-D CFD solutions were determined for the 0, 11, 25, 30, 40 and 45 degree flap angle settings. The losses from the test were computed on a mass averaged basis. The mass averaged total pressure loss was determined by the following equation

$$\bar{P}_t(r) = \frac{\int_{\theta_1}^{\theta_n} P_t \rho U r d\theta}{\int_{\theta_1}^{\theta_n} \rho U r d\theta} \quad (1)$$

where U is the local axial velocity, and ρ is the density. Where P_t is the total pressure measured behind the inlet guide vane, r is the radial coordinate, θ is the circumferential or pitchwise direction of the flow survey. The loss was integrated over a 72 degree sector.

The mass average loss $\bar{\omega}$ was computed by

$$\bar{\omega} = \frac{P_0 - \bar{P}_t}{P_0 - P} \quad (2)$$

where P_0 is the inlet total pressure measured at the plenum, and P is the static pressure ahead of the IGV.

For the 3-D solution the total pressure was obtain by mass averaging the total enthalpy, density, and velocities to compute the total pressure at an axial grid line downstream of the IGV. The mass averaged quantities are computed as

$$\bar{\rho} = \frac{\overline{\rho u}}{\bar{u}} \quad (3)$$

$$\bar{u} = \frac{1}{\dot{m}} \int u d\dot{m} \quad (4)$$

$$\bar{h}_t = \frac{1}{\dot{m}} \int h_t d\dot{m} \quad (5)$$

where $\dot{m}$ is the total mass flow, $d\dot{m}$ is an increment in the mass flow, $\bar{\rho}$ is the mass averaged density, $\bar{u}$ the mass averaged velocity and $\bar{h}_t$ the mass averaged enthalpy. At the inlet or exit plane, the mass averaged total pressure is obtained from the mass averaged enthalpy, velocities, total temperatures and density. The total temperature is computed from

$$\bar{T}_t = \bar{h}_t / c_p \quad (6)$$

where $\bar{T}_t$ is the mass averaged total temperature and c_p is the specific heat of the gas. The mass averaged total pressure becomes

$$\bar{P}_t = \bar{P} \times (\bar{T}_t/\bar{T})^{\gamma/(\gamma-1)} \quad (7)$$

where $\bar{P}$ is the mass averaged static pressure, $\bar{T}$ is the mass averaged static temperature and γ is the specific heat ratio. The mass averaged total pressure is computed at each radial position downstream of the IGV and the loss computed from Equation (2).

For the 2-D solutions, equations (3), (4) and (5) are used plus an additional equation to mass average the entropy.

$$\bar{s} = \frac{1}{\dot{m}} \int s d\dot{m} \quad (8)$$

and

$$\frac{\bar{s}}{c_p} = \ln\left[\frac{h_t}{h_{ti}}\right] \quad (9)$$

$$\bar{h}_{ti} = \bar{h}_t e^{-\bar{s}/c_p} \quad (10)$$

$$\bar{P}_t = (\bar{h}_{ti})^{\gamma/(\gamma-1)} \quad (11)$$

where $\bar{s}$ is the mass averaged entropy, $\bar{h}_{ti}$ is the ideal total enthalpy, and c_p is the specific heat of air.

Thus, the 2-D loss coefficient becomes

$$\bar{\omega}_{2D} = \frac{P_{t1} - \bar{P}_{t2}}{P_{t1} - P_1} \quad (12)$$

where P_{t1} is the inlet total pressure, P_1 is the inlet static pressure and $\bar{P}_{t2}$ is the mass averaged total pressure at the exit of the grid or any axial position downstream of the blade row.

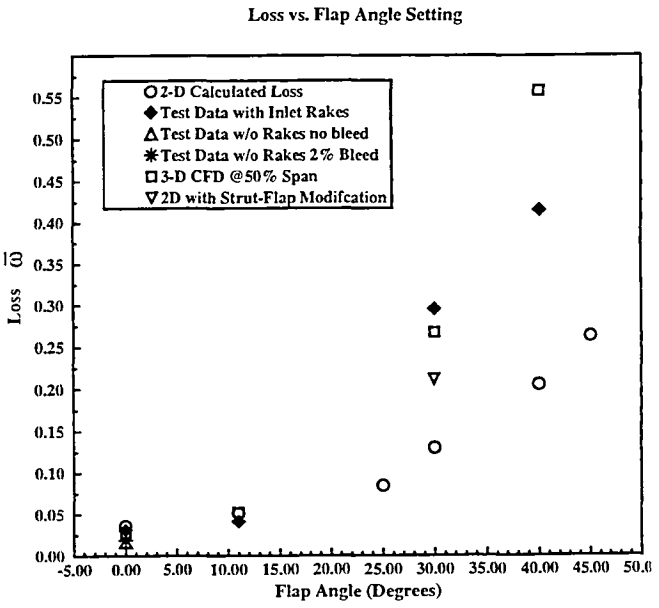

Figure 17. Loss comparisons between the Test, 3-D and 2-D CFD at several flap angle settings

The losses were computed for the test data, 3-D CFD solutions and 2-D blade-to-blade computations at the measurement plane for several flap angle settings. Figure 17 shows the losses compared for the various flap settings. As the loss for the blade-to-blade computations were 2-D, only the losses for the 3-D and the test data at mid-span are represented. At the zero degree flap angle setting, the test losses were also shown with and without bleed and with and without the inlet rake ahead of the IGV. The 2-D and 3-D loss values were quite comparable to the test data at the lower flap angles.

For the 2-D loss correlation verses the flap angle setting, the variation of the loss increased smoothly, but, the losses were substantially lower than what had been measured at the higher flap angles. What is significant about the loss was the sudden increase at the 30 degree flap angle setting in the test data. The 2-D calculated loss was half of the test result. The 2-D model was modified as a strut-flap combination, which increased the loss levels from 0.13 to 0.21, however, it was still lower than the measured loss, but in the right direction. As mentioned earlier, the 3-D solution was then allowed to leak flow between the strut and flap portion of the IGV at the higher flap angles. The loss for the 3-D computation compared fairly well to the measured loss in the test. The losses

increased significantly due to leakage flow between the strut and the flap, which produced a suction side separation on the flap driving the losses considerably higher. The measured loss also included loss from the inlet rakes ahead of the IGV which would produce a higher loss than what was computed. Notice at 40 degrees, the 3-D computed loss was actually higher, this was due to using a coarser axial grid and allowing too much leakage flow producing a larger separation, hence, the CFD losses are higher than the measure values.

The was a significant finding. The losses could probably be reduced by placing a seal between the strut portion of the IGV and the flap. The losses would probably still be higher than the 2-D baseline losses, but definitely much lower than what was previously measured in the test. This is extremely important to improve the off-design performance.

3.5 3-D CFD compared to Test

From Part I, radial and circumferential surveys were taken behind the inlet guide vane with a miniature traversing cobra probe. Comparisons with the 3-D CFD computations are made at 0, 11, 30, and 40 degree flap angle settings. As the flap angle changes, a clearance developed over the ends of the flap. The clearance was modeled by allowing leakage flow over the first 3 grid points near the hub and the last 3 grid points near the casing only over the flap portion of the grid. At the higher flap angles, the flow was also allowed to leak between the strut and the flap.

To reiterate, the 3-D CFD solutions were computed without the inlet rakes or the main support strut just ahead of the IGV. From Figure 18, the comparison of the total pressure contours between the test data and the 3-D CFD calculation are in fairly good agreement at the zero degree flap angle setting and 0% boundary layer bleed. The wakes shed from the IGV's are relatively thin. The hub and casing boundary layers in the CFD computation appear slightly thinner than the measured boundary layers. The interaction of the probe with the boundary layer introducing additional blockage and attributing the lower total pressure measure during the test. In general, the CFD comparison was fairly good, however, at the zero degree flap angle setting, not much secondary flow features or clearance effects are present in the flow field. Thus, the 3-D solution compared fairly well to the measured test data.

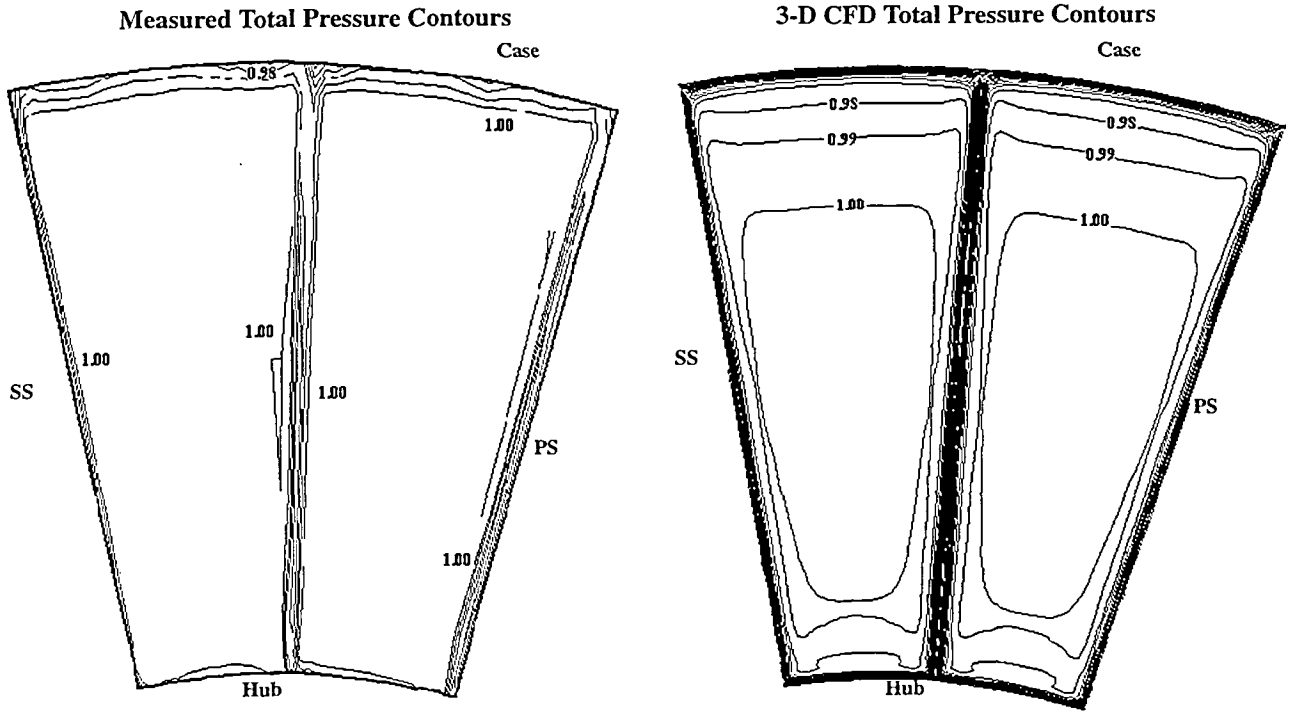

Figure 18. Comparisons of the Total Pressure Contours At the Measurement Plane between the Test and the 3-D Computation at Zero Degree Flap Angle Setting and 0% Bleed

The off-design performance was important to the operation of the compressor, which would be installed behind the inlet, thus, the CFD computations were made at three other flap angle settings. At the 11 degree flap angle setting, the test data was also obtained with 1% boundary layer bleed. For the CFD solution, the flap was set to 11 degrees closed, the boundary layer bleed was set to 1% of the flow and flow was allowed to leak through the clearance over the flap.

Figure 19 shows a comparison between the test data and the CFD computation at the 11 degree flap setting. There was very little resolution of the boundary layer in the test data at this flap setting. Ignoring the region where the inlet rake existed, the rest of the test data indicated fairly thin wakes behind the IGV at this flap setting. Near the hub, the appearance of a small clearance vortex forming can be seen. From the CFD solution, the wakes are still relatively thin as well as the hub and casing boundary layers. The computation clearly indicated two clearance vortices have formed, one near the hub and the other near the casing. The vortices are slightly askew from the main IGV wake structure. As the flow is turned, the wakes are turned at the same flow angle as the flap angle; but the clearance flow had spilled over the flap from the pressure side of the blade to the suction side creating a clearance vortex at a much reduced flow angle. Even though the test data didn't have much casing boundary layer data, the solutions agreed qualitatively. The wakes are just slightly larger in the CFD computation, however, the test data at this particular flow angle was relatively sparse so it was difficult to determine the quantitative accuracy of the results. The 3-D CFD solution slightly over predicted the losses.

For any higher flap angle setting, the computation would be modeled by allowing flow to leak between the strut and the flap as well as allowing for the clearance over the flap. The measured data captured the wakes off of the inlet rakes upstream of the IGV which combined with the wake from IGV. This produced a slightly larger wake profile than the measured values on either side of it. In the next two figures, Figures 20 and 21, the measured data at 30 and 40 degree IGV flap angle settings are compared to the CFD computations. These comparison are made to the wakes strictly generated by the IGV and not the wake which has the rake wake included.

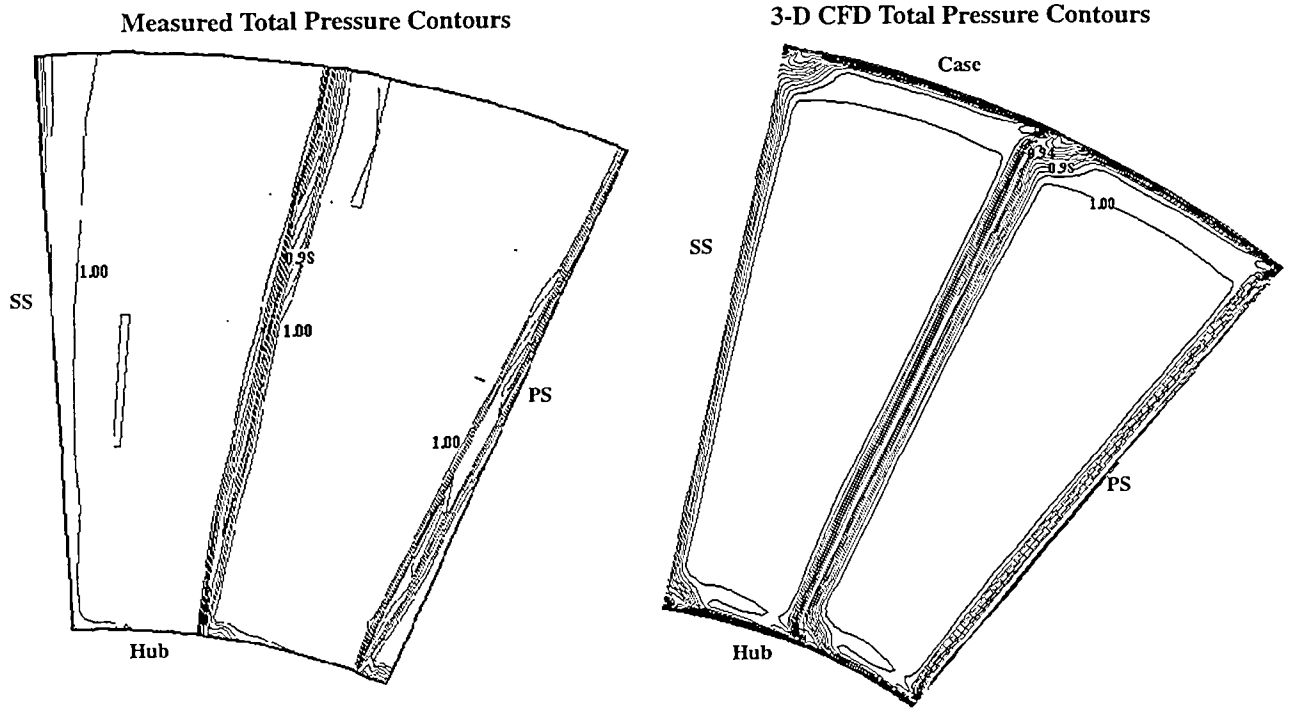

Figure 19. Comparisons of the Total Pressure Contours at the Measurement Plane between the Test and the 3-D Computation at 11 Degrees Flap Angle Setting and 1% Bleed

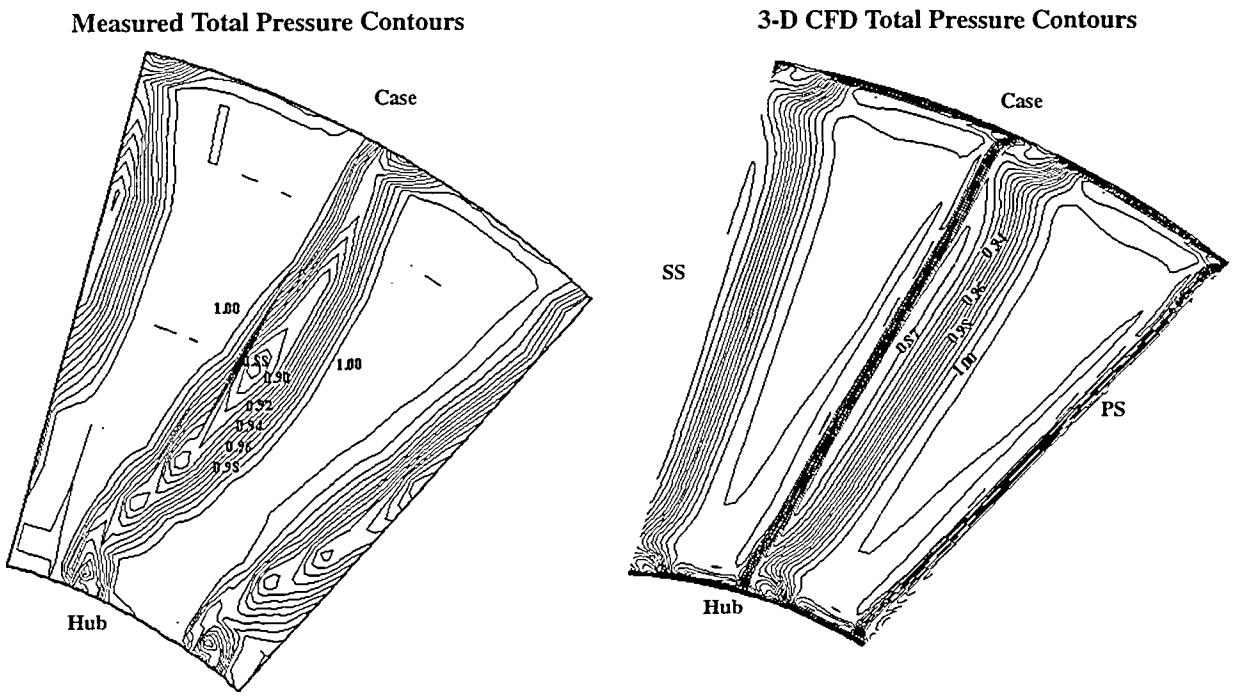

Figure 20. Total Pressure Contours of the Test and the 3-D CFD at 30 Degree IGV Flap Angle

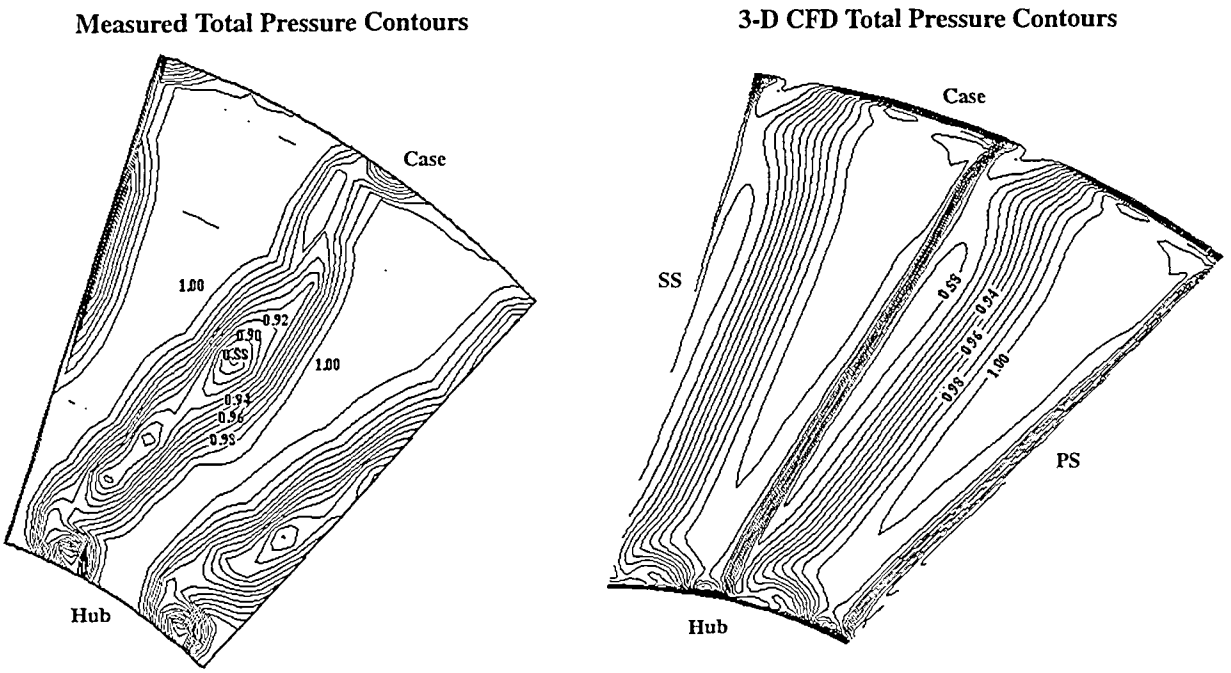

Figure 21. Total Pressure Contours of the Test and the 3-D CFD at 40 Degree IGV Flap Angle

Qualitatively the results looked comparable. The clearance vortices are similar in magnitude and direction. The quantitative differences are in the detailed wake structure. The test data showed localized lower total pressure areas in the wake of the airfoil whereas the total pressure was more distributed through out the entire span of the blade in the CFD solutions. This was probably due to localized separated regions of the airfoil due to non-uniform gap leakage in the test which produced higher local flows through the gap, whereas the CFD model used a uniform gap leakage. At 40 degrees, the computed wake had more leakage flow than in the test. Even though the model allowed too much leakage flow through the gap, the qualitatively results are fairly good.

4.0 Concluding Remarks

A compressor inlet was designed and tested in SECTF facility at NASA Lewis Research Center to verify inlet conditions for a small axial compressor. Detailed flowfield measurements were obtained using a miniature traversing cobra probe and the measured data compared to CFD results using ADPAC, which is a four stage Runge-Kutta finite volume multi-block Navier-Stokes flow solver. The flow measurements were taken over several different flow conditions and IGV setting angles with and without bleed.

Three sets of Comparisons were made between the CFD and the test results. The first part looked at the comparisons of the axisymmetric throughflow and 3-D CFD analysis to the test. For zero degree flap angle and zero percent boundary layer bleed, very good agreements were achieved between the measured data and the CFD solutions. With 2% boundary layer bleed at the same flap angle, better agreement was seen between the test data and the CFD results. Computed mass flows were found to be within 1% error between the CFD and the test data, which is within the measurement error for the test.

Good agreements were obtained from the 2-D blade-to-blade CFD solutions compared to the mid-span 3-D CFD computations. The most significant finding was discovered from the modification of the computational models to predict the losses observed at fairly high flap angle settings. To achieve the high losses obtained from the test, the model was constructed in such a way as to leak flow between the strut and the flap portion of the IGV. The loss agreement at the 30 degree flap setting between the 3-D CFD solution and the test data were fairly close. Therefore, there must have been leakage flow between the strut and flap during the original testing of the inlet. An improvement can be made by placing a seal between the strut and the flap improving the off-design performance of the IGV. The CFD analysis has become an effective tool for predicting off-design performance.

In comparing the 3-D CFD solutions to the measured radial and circumferential traverse downstream of the IGV, fairly good agreement was observed between the CFD results and the survey. For 11, 30 and 40 degree flap angles, the clearance flows were added to the computational model which captured the clearance vortices forming near the hub and casing as was seen from the data. Qualitatively, the 3-D CFD results captured the flow physics downstream of the IGV. The pressure magnitudes appear fairly close to the measured values. The exceptions are the quantitative results, where localized losses were higher as observed from the test data. There could have been localized separations on the airfoil where as the CFD model computed a more uniform separation of the flow. The CFD provided a valuable insight into the test data. ADPAC is an excellent CFD tool which can be used to solve complex flow problems.

5.0 Acknowledgments

The author(s) would like to thank the following personnel for contributions to this program: Kevin McCormick and Charlie Martin for assembly and operation of the test hardware. Richard Brokopp, Teresa Gibson and Bob Gronski for maintaining and operating the facility. Bill Stevans for his contribution on the design of a ring traverse probe. Sue Prahst, co-author, for writing the data reduction program. Finally, Chris Miller for his timely advice on the operation and running of ADPAC.

6.0 References

[1] Brokopp, R. A. and Gronski, R. S., "Small Engine Components Test Facility Compressor Testing Cell at NASA Lewis Research Center" NASA TM-105685, Presented at the 17th AIAA Aerospace Ground Testing Conference, Nashville, TN, July 1992, pp. 1-11.

[2] Miller, D.P., and Prahst, P.S., "Inlet Flow Test Calibration for a Small Axial Compressor Facility Part I - Design and Experimental Results" NASA TM-106719, June 1994.

[3] Hall, E. J., Delaney, R. A., and Bettner, J. L., "Investigation of Advanced Counterrotation Blade Configuration Concepts for High Speed

Turboprop Systems; Task I - Ducted Propfan Analysis Final Report". NASA CR-185217, Contract NAS3-25270, April 1990.

[4] Hall, E. J., Delaney, R. A., and Bettner, J. L., "Investigation of Advanced Counterrotation Blade Configuration Concepts for High Speed Turboprop Systems; Task II - Unsteady Ducted Propfan Analysis, Final Report." NASA CR-187106, Contract NAS3-25270, May 1991.

[5] Hall, E. J. and Delaney, R. A., "Investigation of Advanced Counterrotation Blade Configuration Concepts for High Speed Turboprop Systems; Task V - Unsteady Counterrotation Ducted Propfan Analysis, Final Report". NASA CR-187126, Contract NAS3-25270, January, 1993.

[6] Hall, E. J., Topp, D. A., Heidegger, N. J., and Delaney, R. A., "Investigation of Advanced Counterrotation Blade Configuration Concepts for High Speed Turboprop Systems; Task VIII - Cooling Flow/ Heat Transfer Analysis, Final Report". NASA CR-195359, Contract NAS3-25270, September, 1994.

[7] Hall, E. J., Topp, D. A., Heidegger, N. J., and Delaney, R. A., "Investigation of Advanced Counterrotation Blade Configuration Concepts for High Speed Turboprop Systems; Task VIII - Cooling Flow/ Heat Transfer Analysis, User's Manual". NASA CR-195360, Contract NAS3-25270, September, 1994.

[8] Miller, D. P., "TIGGERC-Turbomachinery Interactive Grid Generator for 2-D Grid Applications and Users Guide", NASA TM 106586, May 1994.

[9] Crook, A. J. and Delaney, R. A., "Investigation of Advanced Counterrotation Blade Configuration for High Speed Turboprop Systems; Task III - Advanced Fan Section Grid Generator, Final Report and Computer Program User's Manual", NASA CR-187129, Contract NAS3-25270, September 1991.

REPORT DOCUMENTATION PAGE

Form Approved
OMB No. 0704-0188

1. AGENCY USE ONLY (*Leave blank*)	2. REPORT DATE	3. REPORT TYPE AND DATES COVERED
	July 1995	Technical Memorandum

4. TITLE AND SUBTITLE
Inlet Flow Test Calibration for a Small Axial Compressor Rig: Part II. CFD Compared With Experimental Results

5. FUNDING NUMBERS
WU-505-62-10

6. AUTHOR(S)
D.P. Miller and P.S. Prahst

7. PERFORMING ORGANIZATION NAME(S) AND ADDRESS(ES)
National Aeronautics and Space Administration
Lewis Research Center
Cleveland, Ohio 44135-3191

8. PERFORMING ORGANIZATION REPORT NUMBER
E-9778

9. SPONSORING/MONITORING AGENCY NAME(S) AND ADDRESS(ES)
National Aeronautics and Space Administration
Washington, D.C. 20546-0001

10. SPONSORING/MONITORING AGENCY REPORT NUMBER
NASA TM-106999
AIAA-95-3037

11. SUPPLEMENTARY NOTES
Prepared for the 31st Joint Propulsion Conference and Exhibit cosponsored by AIAA, ASME, SAE, and ASEE, San Diego, California, July 10-12, 1995. D.P Miller, NASA Lewis Research Center and P.S.Prahst, NYMA Inc., 2001 Aerospace Parkway, Brook Park, Ohio 44142. Responsible person, D.P. Miller, organization code 2760, (216) 433-8352.

12a. DISTRIBUTION/AVAILABILITY STATEMENT
Unclassified - Unlimited
Subject Category 07

This publication is available from the NASA Center for Aerospace Information, (301) 621-0390.

12b. DISTRIBUTION CODE

13. ABSTRACT (*Maximum 200 words*)

An axial compressor test rig has been designed for the operation of small turbomachines. A flow test was run to calibrate and determine the source and magnitudes of the loss mechanisms in the compressor inlet for a highly loaded two-stage axial compressor test. Several flow conditions and IGV angle settings were established, which detailed surveys were completed. Boundary layer bleed was also provided along the casing of the inlet behind the support struts and ahead of the IGV. Several CFD calculations were made for selected flow conditions established during the test. Good agreement between the CFD and test data were obtained for these test conditions.

14. SUBJECT TERMS	15. NUMBER OF PAGES
Turbomachinery; Compressor; CFD; Loss sources	16
	16. PRICE CODE: A03

17. SECURITY CLASSIFICATION OF REPORT	18. SECURITY CLASSIFICATION OF THIS PAGE	19. SECURITY CLASSIFICATION OF ABSTRACT	20. LIMITATION OF ABSTRACT
Unclassified	Unclassified	Unclassified	

National Aeronautics and
Space Administration

Lewis Research Center
21000 Brookpark Rd.
Cleveland, OH 44135-3191